Geophys. J. Int. (2004) **157,** 1206–1216 doi: 10.1111/j.1365-246X.2004.02268.x

Imaging of complex basin structures with the common reflection surface (CRS) stack method

Elive Menyoli, Dirk Gajewski and Christian Hübscher

Institute of Geophysics, University of Hamburg, Bundesstrasse 55, D-20146 *Germany. E-mail: gajewski@dkrz.de (DG)*

Accepted 2004 January 27. Received 2004 January 23; in original form 2003 April 25

SUMMARY

Common reflection surface (CRS) stack technology is applied to seismic data from certain areas of the Donbas Foldbelt, Ukraine, after conventional seismic methods gave unsatisfactory results. On the conventionally processed post-stack migrated section the areas of interest already showed clear features of the basin structure, but reflector continuity and image quality were poor. It was our objective to improve the image quality in these areas to better support the geological interpretation and the model building.

In contrast to the standard common mid-point (CMP) stack, in which a stacking trajectory is used, the CRS method transforms pre-processed multicoverage data into a zero-offset section by summing along stacking surfaces. The stacking operator is an approximation of the reflection response of a curved interface in an inhomogeneous medium. The primary advantage of the data-driven CRS stack method is its model independence and the enhancement of the signal-to-noise ratio of the stacked sections through a stacking reflection response along traces from more than one CMP gather. The presented results show that the multifold strength of the CRS stack is of particular advantage in the case of complex inverted features of Devonian–Carboniferous sediments in the Donbas Foldbelt data. We observe that in these areas where the confidence level for picking and interpretation of the stacking velocity model is low, imaging without a macrovelocity model gives improved results, because errors due to wrong or poor stacking velocity models are avoided.

Key words: common reflection surface stack, foldbelt, inverted structures.

1 INTRODUCTION

In the framework of the DOBREflection 2000 project (DOBREflection 2000) a 140 km 2-D seismic line was acquired across the Donbas Foldbelt (DF) by Ukrgeofisika (a Ukrainian national oil company) and reprocessed at the University of Hamburg, Germany. The objective of the project was to investigate the interplay of the geological and geodynamic processes that controlled the evolution of the DF as an example of an inverted intracratonic rift basin (Stovba *et al.* 1996; Maystrenko *et al.* 2003). Despite the generally good quality of the DF data set, in some areas structural features which show the extent of the basin inversion were poorly imaged in the conventionally post-stack time-migrated section. In these areas the imaging potential of the post-stack migration was limited by the quality of the stacked section. Reflectors are not visible due to a low signal-to-noise (S/N) ratio, and in other areas their continuity was disrupted. Therefore, it was difficult to trace fault systems from the surface to greater depths. Likewise, in the deeper areas a low S/N ratio resulted in poor images.

We attribute the poor imaging to the complexity of thrust faulting and folding of Palaeozoic and younger sedimentary layers. Thrust faulting and folding produces locally very steep dips and strong lateral velocity variations, thus violating the assumption of common reflection point traces which is used in conventional common mid-point (CMP) stacking (Yilmaz 2001; Yan & Line 2001). In foldbelt areas conventional seismic methods such as normal moveout (NMO)/dip moveout (DMO) stacking often also give unsatisfactory imaging results. In order to improve the image quality of the key areas we used the zero-offset common reflection surface (CRS) stack method (Müller 1998, 1999; Mann *et al.* 1999; Perroud *et al.* 1999; Jäger *et al.* 2001; Menyoli *et al.* 2002) which like multifocusing (Gelchinsky & Keydar 1999; Gelchinsky *et al.* 1999; Landa *et al.* 1999) belongs to the group of macro model-independent imaging tools.

The CRS stack is a new alternative to the classical processing sequence of normal moveout, dip moveout and stacking. The method uses a stacking operator that locally describes the response of a reflector in a laterally inhomogeneous medium and does not depend on the interpretation of a stacking velocity model (Mann *et al.* 1999). Using real data sets, Mann *et al.* (1999) and later Trappe *et al.* (2001) demonstrated the strength of CRS stacking. In contrast to the classical CMP stacking operator which requires only one parameter (the stacking velocity model), the CRS operator uses three parameters. These parameters are associated with the wave fronts of the so-called

'eigenwaves' and are used to account for the local properties of the subsurface interfaces (Hubral & Krey 1980; Hubral 1983).

This technique found several application in the exploration industry and was primarily used in the context of hydrocarbon exploration. The potential for general geoscientific studies like, for example, basin evolution and dynamics or crustal studies, had not been developed. Here we apply the CRS stacking method to the Donbas Foldbelt data and show that in contrast to the conventionally stacked section, the image quality of the significant structures of the inverted basin is greatly improved. The obtained high-quality image strongly supported the geological interpretation and the model building process as well as the palinspastic reconstruction (for details we refer to Maystrenko *et al.* 2003, where, however, no CRS results are shown or discussed). Before passing the data set into the CRS stack algorithm detailed pre-processing and noise analysis was required since the success of any seismic imaging method depends on the quality of the pre-processed data. To suppress diffraction events of the ZO sections post-stack time migration was applied after the stack.

First, we will describe the geological setting of the Donbas Foldbelt area and then the pre-processing steps that where chosen in order to suppress noise and unwanted signals. This will be followed by a review of the CRS stack method and its application to the foldbelt seismic data.

2 LOCATION AND GEOLOGICAL SETTING

The Donbas Foldbelt (DF) is the uplifted and compressionally deformed eastern part of the Late Palaeozoic Dniepr-Donets rift basin, located in southeastern Ukraine. The Dniepr-Donets Basin (DDB) generally strikes in the northwest–southeast direction and divides the Eastern European Craton into the Ukrainian Shield and the Voronezh High (Fig. 1). The DDB is usually divided into three main parts, including the relatively shallow Pripyat Basin with a maximum sedimentary infill of about 4 km, the deeper central Dniepr-Donets Basin with sedimentary fill of up to about 20 km and the uplifted and strongly inverted Donbas Foldbelt (Stovba & Stephenson 1999; Maystrenko *et al.* 2003).

The sedimentary successions within the DDB are mostly Late Devonian syn-rift and Carboniferous–Palaeogene post-rift successions. The DDB developed and evolved as a result of rifting and lithospheric extension (Chekunov *et al.* 1992; Stovba & Stephenson 1999; Maystrenko *et al.* 2003). Rapid syn-rift subsidence occurred during lithospheric extension as the result of crystal thinning induced by lithospheric geothermal increase. After the main rifting stage in the Late Devonian, extension and rift reactivation plus uplifting started in the Lower Carboniferous (Stovba & Stephenson 1999). This was followed by post-rift subsidence in the Middle Carboniferous. Uplifting and extension regained strength in Permian–Jurassic times. In Early Permian times the DF was highly uplifted and compressed compared with the central and northeastern part of the basin. Folding, thrusting and reverse faulting mainly occurred in Late Cretaceous–Tertiary times. The strong inversion, which was more pronounced in the DF region, caused serious deformation in the sedimentary structures. Likewise, uplifting led to erosion of Permian–Jurassic as well as Cenozoic sediments; thus the main sediments which outcrop at the surface in the DF region are mainly of Carboniferous age (see Fig. 2). To elucidate the evolution of processes that occurred during rifting and rift reactivation, basin uplift and inversion, a seismic profile was acquired.

2.1 Acquisition and data set

The acquisition parameters for the Vibroseis line are illustrated in Table 1. The acquisition started in 2000 June and ended in 2000 September. Detailed quality control in the field was performed by the University of Hamburg and Ukrgeofisika. Important considerations in the acquisition programme included high-fold, long

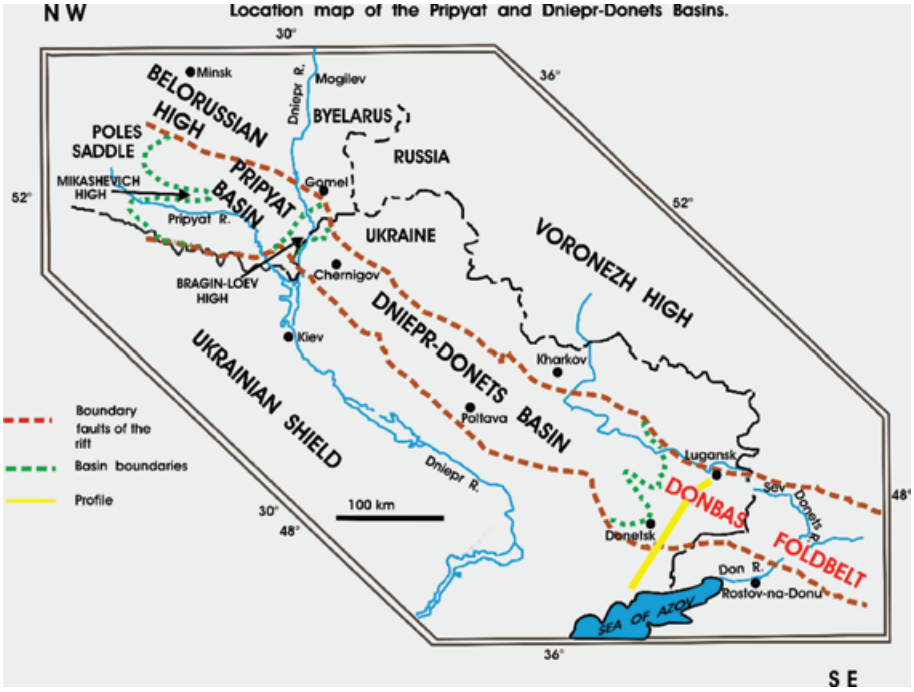

Figure 1. Location map of the survey area with major tectonic zones of the Dniepr-Donets Basin.

Table 1. Seismic data acquisition parameters. S.P. stands for shot point.

RECORDING DATA

Record length	30 s
Sampling interval	2 ms
Channels	681
Geophone/Group	12
Gephone–Frequency	10 Hz

SPREAD

Type	split spread
Number of stations	681
Station interval	35 m
Minimum offset	35 m
Maximum offset	12000 m

VIBROSEIS PATTERN

Number of vibrators	4
Sweep frequency	8–80 Hz
Sweep length	12 s
Sweep type	linear
S.P. position	on half station
S.P. interval	140 m
Coverage	85 fold
Number of vert. stack/V.P.	20
Recording length	30 s

SPREAD DIAGRAM

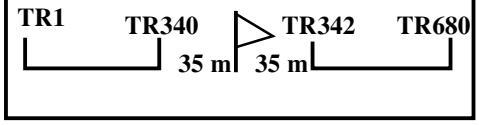

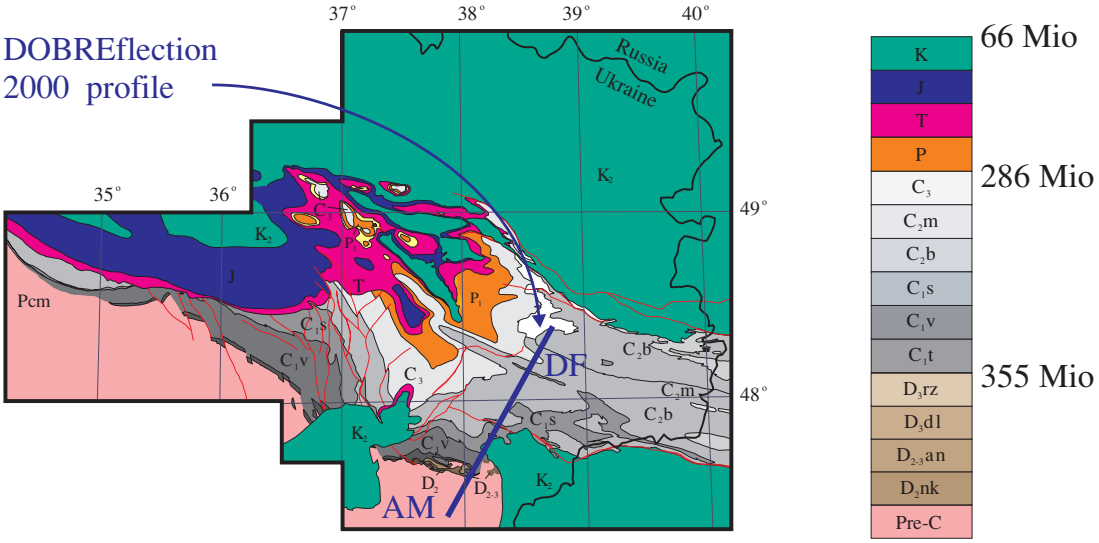

Figure 2. Cenozoic subcrop map of the central part of the Dniepr-Donets Basin and the Donbas Foldbelt (DF). AM is the Azov Massif, and the thick blue line indicates the DOBREflection-2000 profile.

receiver array lengths and an offset range that corresponds to an angle of incidence from 0 to 45° according to the deepest target event. The area of the survey was 140 km and a total of 877 Vibroseis shot records were acquired with an average shot spacing interval of 140 m. The shot interval was not always constant along the profile: in some areas there were shot point gaps due to prohibition of shooting operations within an extensive network of coal mining. Each shot gather was made up of 680 traces with a geophone spacing of 35 m. The acquisition geometry was mainly a split-spread configuration, apart from some areas where an asymmetric split-spread and end-on spread configuration was used. The nearest and largest offsets on most shot records were 35 m and 12 000 m respectively for each side of the spread (for the end-on spread it was 35 m and 24 000 m). The central parts of the survey had a coverage of 84-fold. Many of the traces that contribute to the fold diagram were from very large offsets. Low-fold areas were found to be more susceptible to local noise problems (such as poor geophone coupling and spurious traces) than high-fold areas. The low-fold areas generally produce regions with lower amplitude in the stacked sections. The lack of a uniform distribution, which was related to the patch acquisition, was recognized as a problem and degraded the results in some areas. Also included in the database was a surface structural geological cross-section coincident with the path of the seismic line (Fig. 2).

3 PRE-PROCESSING

The data had a maximum frequency of 120 Hz with a central frequency close to 30 Hz. The processing parameters were mostly space-variant, i.e. the parameters were often adjusted along the profile in response to the continuously changing quality of the data. This is very common for onshore data. Special attention was given to preserve the large frequency bandwidth at all stages of the

processing. To increase the signal in the seismogram, a gain function with a large window was applied (automatic gain control (AGC) 3000 ms). With this large AGC window the amplitude character of the genuine reflection events was not seriously damaged. In order to increase the S/N ratio and to suppress coherent surface waves the following standard processing steps were applied: trace editing and noise analysis, spherical divergence correction, surface-consistent deconvolution, spectral balancing and residual static corrections. Trace editing included the removal of bad traces, dead traces and polarity reversal on each shot gather. We used the criteria that a good trace exhibit amplitude and frequency decay with time while a bad trace is one that manifests a constant amplitude status and frequency content with time.

The next processing step involved muting the direct waves and first arrivals from refractions. The mute window was specified separately for each shot with special care taken in order to preserve reflections from steeply dipping horizons. Due to the complex tectonic setting (steep-dipping horizons and overthrusting), the apex of some reflection hyperbolas was shifted towards the first arrivals in the shot gather. The process of muting was followed by the application of a geometrical spreading correction and an exponential gain function. The geometrical spreading correction is expressed as a function of subsurface velocity and traveltime. The average subsurface velocity was estimated and supplied by Ukrgeofiska. After a set of tests, a suitable geometrical spreading function of $v^2t^{3/2}$ was chosen. Next, the trace amplitudes were balanced on a record basis using trace equalization. This was accomplished by scaling the data to a defined energy level. For each trace a separate balancing factor was computed. This factor was applied individually to each trace, thereby keeping relative amplitudes throughout the trace. We used a time-variant high-pass filter (low-cut) to first suppress the low-frequency components of the data. A broad-band trapezoid filter of 3/5–80/100 Hz was later applied to suppress the high-frequency component of the signal. The next major processing steps were surface-consistent deconvolution and spectral balancing. However, before passing the Vibroseis data to deconvolution, the data had to be transformed to their minimum phase counterpart. The minimum delay transformation is performed following a strategy described by Fertig *et al.* (1999). The process of minimum delay transformation was followed by surface-consistent spiking deconvolution with an operator length of 128 ms and white noise of 0.1 per cent. The parameters, e.g. the frequency band, were chosen based on the resulting character of the deconvolved data. Filters for unspecified shot ensembles and traces were defined by spatial interpolation. Because both high-frequency noise and signals were boosted after deconvolution, the data were later filtered with a bandpass filter of 8/10–40/60 Hz.

Fig. 3 shows the first 3 s of an example shot gather before processing and Fig. 4 shows the same shot gather after processing. In Fig. 4 the surface waves, high-frequency signals at zero offset and first arrival refractions are all suppressed. These figures demonstrate that the objective of enhancing the genuine reflection signals by suppressing coherent and random noise was well achieved. After pre-processing the shot gathers were sorted to CMP gathers and were input into conventional stacking velocity analysis, stacking and post-stack time migration. Fig. 5 shows the Kirchhoff post-stack time-migrated section of the whole line up to the two-way time of 15 s. Note that for display purpose only every 10th trace is plotted. The zones with no data were due to lack of shot points in these areas as a result of mining activities. The root-mean-square (rms)

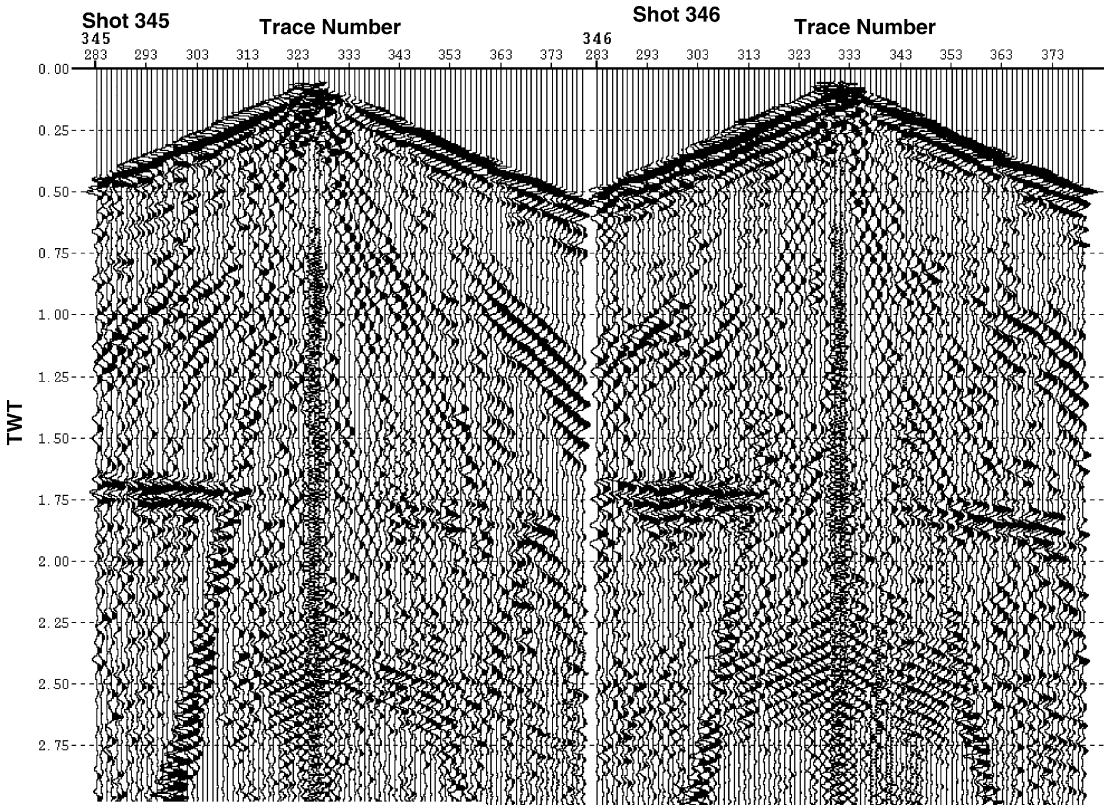

Figure 3. Split spread shot gathers of the Vibroseis survey. The gathers correspond to shot numbers 345 and 346 before pre-processing. An AGC with a time window of 1000 ms was applied for display. For shot 345 the source is located between channel 325 and 326 and for shot 346 the source is located between channel 331 and 332.

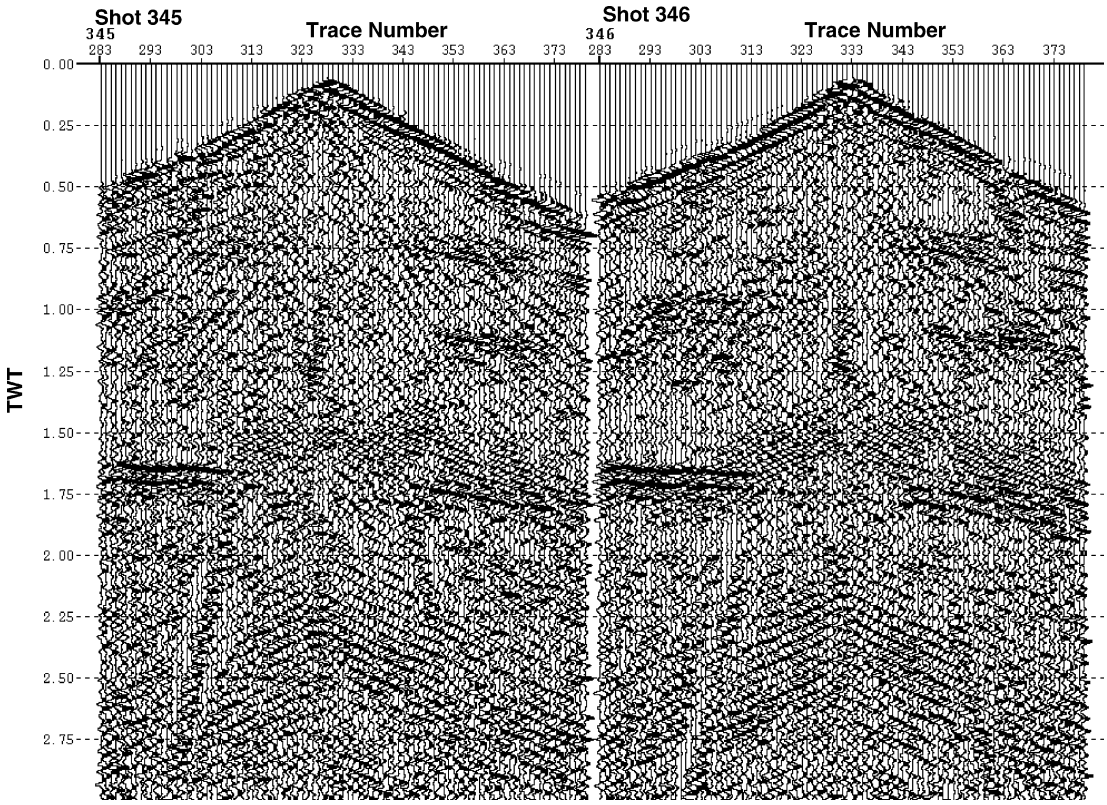

Figure 4. Same shot gathers as in Fig. 3 after pre-processing. Notice the reduction of the surface waves and of the high-frequency noise in the centre.

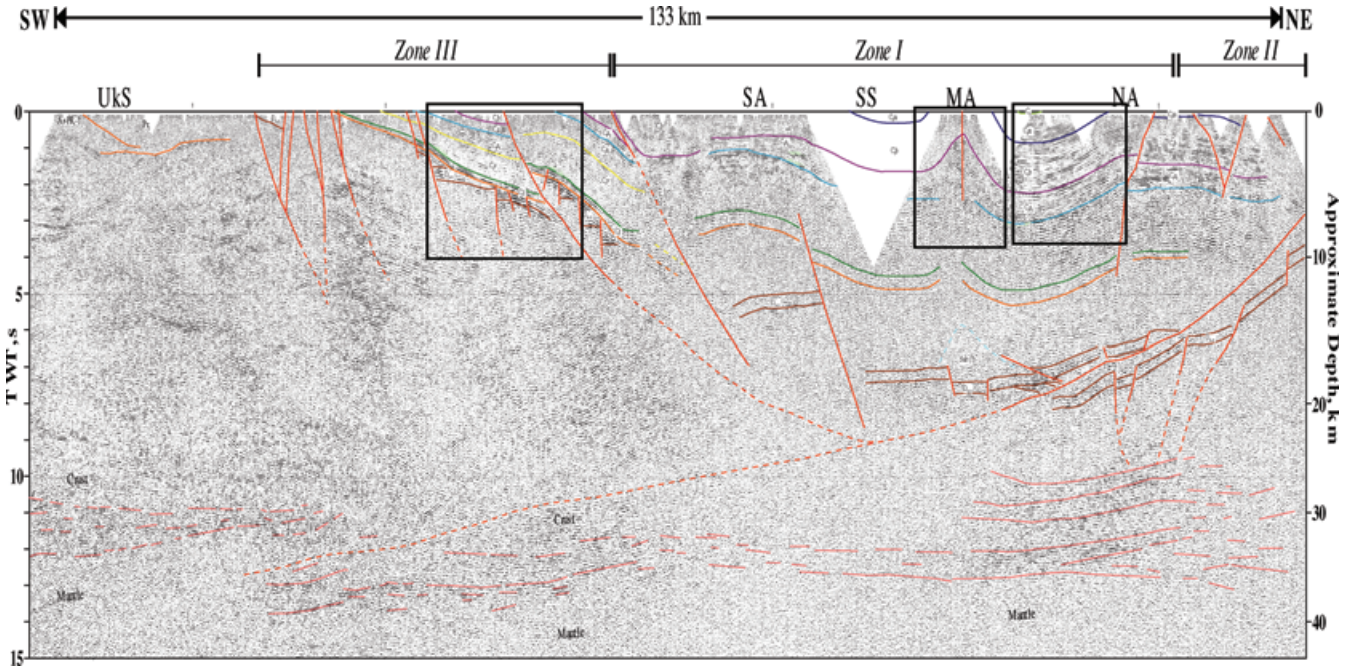

Figure 5. Interpreted post-stack time migration of the seismic line. This interpretation was constrained using surface structural geology information. The boxes show three areas to be imaged with the CRS stack algorithm.

velocities used for post-stack time migration were derived from the stacking velocities. The rms velocities were later modified to give the optimum time migrated section.

Generally Fig. 5 reveals a detailed image of the sedimentary basin with folding and faulting patterns. The sedimentary cover is expressed as a well-defined package of reflectors. The sediments are resolved from the Ukrainian Shield (Zone III) to the axial part of the DF (Zone I) and further towards the northern part (Zone II) of thrusting and folding. Despite the generally good image quality of the migrated section, several key structural features of the section were unsatisfactorily imaged. These areas are indicated by the boxes in Fig. 5. In these areas some main reflectors are disrupted

and their continuity is unclear. Uncertain reflector continuity can lead to incorrect geological interpretation, e.g. incorrect amount of inversion. The continuation of the fault systems from the surface down to the subsurface was poorly delineated. In deeper areas of the basin (two-way traveltime 5–10 s) where the S/N ratio was generally poor geological interpretation of the main horizons was even more complicated. These imaging problems are common in foldbelt data. The imaging problems are not only significant for the geological interpretation but also for the model building which relies on high-quality stacks. In the next section we discuss possible reasons for the poor image quality of CMP stacks in foldbelt areas.

4 IMAGING PROBLEMS IN THE FOLDBELT AREA

Seismic imaging in complex areas such as thrust belts and areas of complex tectonics is hampered by several factors that often lead to poor-quality data. Usually thrust faulting and folding produce locally very steep dips and strong lateral variations in velocity. Fig. 6 (top) is a blow-up of one of the poorly imaged areas in Fig. 5 after applying conventional CMP stacking and post-stack time migration. This fragment of the line shows a basement involving backthrust on the southern flank of the DF as an example of the inversion tectonics. However, only the main reflector is properly imaged. Other minor dipping reflectors are poorly imaged. From the surface structural geological model of this area steeply dipping layers outcrop at the surface, therefore producing strong lateral variations in velocity and out-of-plane reflections. Such steep dipping events and the lateral velocity variations are problematic for conventional CMP stacking and post-stack migration. First of all the assumption of having common reflection point (CRP) traces in CMP gathers is violated and the picking of reflection events during stacking velocity analysis is difficult and tedious. The reflected waves from different reflection points will lead to a poorly interpreted stacking velocity field. A poorly interpreted stacking velocity field results in failure to optimally stack the data with loss of valuable signal and subsequent mispositioning when the data are migrated afterwards. The poorly stacked images eventually lead to poor post-stack migration results since the success of post-stack migration strongly depends on the quality of the unmigrated stacked section rather than on the accuracy of the migration rms velocity. We anticipate that the poor image quality in Fig. 6 is partly due to the above-mentioned problems. To obviate the above imaging problems, we used the CRS stack method which does not require any stacking velocity model and has a high stacking power. We will first briefly review the method and than apply it to the data of certain key zones of the DFdata.

5 REVIEW OF THE CRS STACK METHOD

The CRS stack method uses a stacking operator that describes the reflection moveout response for inhomogeneous media. In contrast to CMP stacking, the CRS method does not directly depend on the macrostacking velocity model. Mathematically, the stacking surface is based on ray theory and for 2-D it is given as (Mann *et al.* 1999; Jäger *et al.* 2001):

$$t^2(x_m, P) \approx \left(t_0 + \frac{2\sin\alpha_0}{v_0}(x_m - x_0)\right)^2 + \frac{2t_0\cos^2\alpha_0}{v_0}\left(\frac{(x_m - x_0)^2}{R_{\mathrm{N}}} + \frac{h^2}{R_{\mathrm{NIP}}}\right), \quad (1)$$

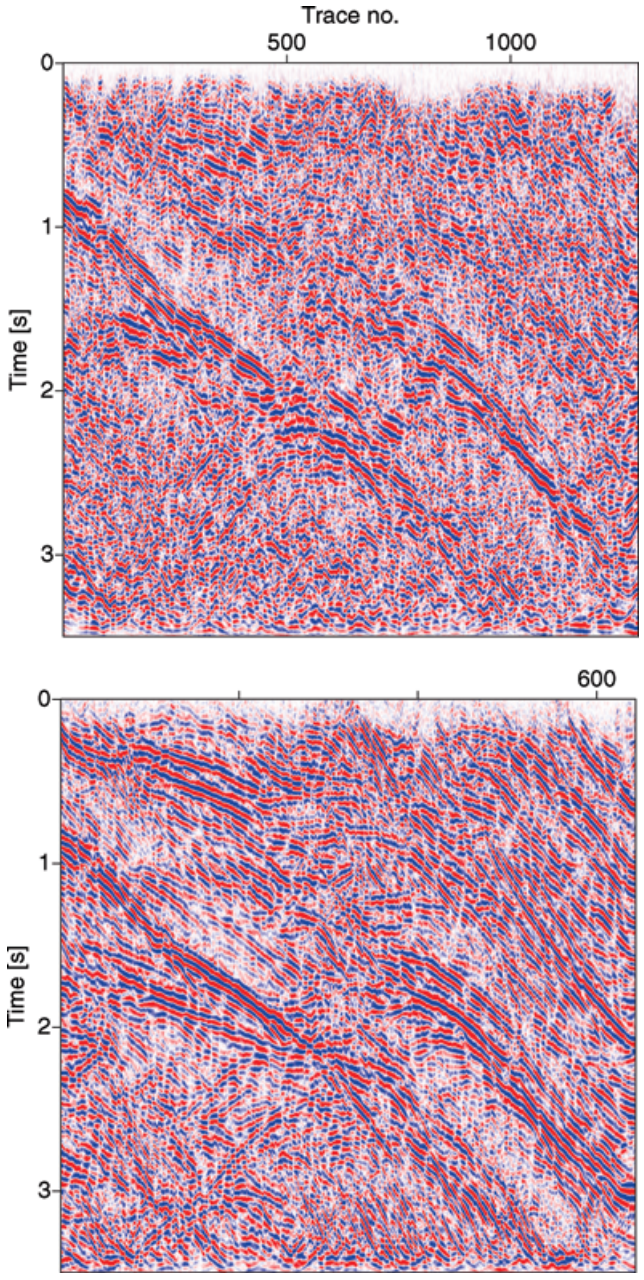

Figure 6. Post-stack time-migrated images after applying conventional CMP stacking (top) and CRS processing (bottom). The images show a backthrust on the southern flank of the DF, i.e. a reverse fault, as an example of the inversion tectonics. Apart from the major reflector which is disrupted by a fault line, other reflectors are poorly imaged in the CMP stack. In the CRS stack (bottom) the change in reflector orientation clearly shows the line of the reverse fault. More dipping reflectors up to the surface are better delineated.

where t is the traveltime, t_0 is the zero-offset traveltime, x_0 is the location of the zero-offset ray on the surface, h is the half-offset between source and receiver and x_m is the mid-point coordinate. The parameters α_0, R_{NIP} and R_{N} are known as the CRS attributes (Hubral & Krey 1980; Jäger *et al.* 2001; Menyoli 2002). Fig. 7 illustrates the three CRS attributes. In eq. (1), R_{NIP} describes the radius of curvature, at the Earth's surface, of a wave from a point source located at the normal incidence point (NIP) on the reflector surface, while R_{N} is the radius of curvature of a wave from an

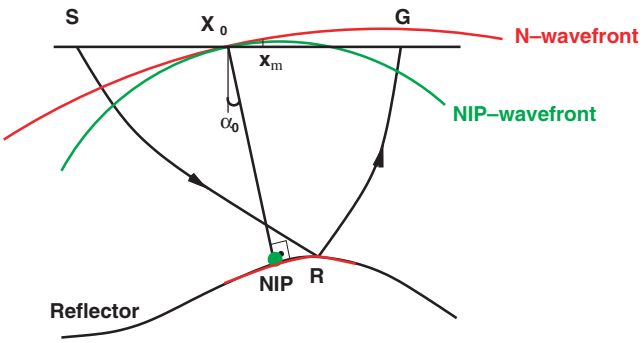

Figure 7. CRS attributes for a normal central ray going from X_0 to NIP and to X_0: the emergence angle α_0 and the NIP and N wave-front curvatures. X_0 is the central point coordinate, and S and G are the source and receiver positions for a ray reflecting at R with the mid-point x_m.

exploding reflector element. The angle, α_0 is the emergence angle at the surface of a ray normal to the subsurface reflector. Note that both the NIP and N wave fronts emerge at the same α_0 on the surface. P abbreviates the dependence of t on h, α_0, $R_{\rm NIP}$ and $R_{\rm N}$. Note that, eq. (1) is equivalent to the conventional CMP stacking operator if $x_m = x_0$. Unlike in conventional stacking, which uses the stacking velocity as the stacking parameter, the wave-front attributes (α_0, $R_{\rm NIP}$, $R_{\rm N}$) are the parameters of the stacking operator. For more details on the attributes and the CRS stacking operator see Hubral & Krey (1980), Jäger *et al.* (2001) and Menyoli (2002).

For each sample (t_0, x_0) in the CRS section to be generated, these attributes are automatically determined via coherence analysis. The only required model parameter is the near-surface velocity v_0. Note that, eq. (1) is analytical and accounts for all shot–receiver pairs with mid-points close to x_0. Therefore, when t_0, x_0 and v_0 are given, the three wave-front attributes are determined by a three-parametric coherence-maximization process. Coherence analysis along various test stacking operators is performed for each particular zero-offset sample to be generated. The stacking operator (and its three wave-front attributes) yielding the highest coherence is used to perform the final stack.

In order to search for the wave-front attributes, Müller (1998) and Jäger *et al.* (2001) proposed a three one-parametric search strategy as shown in Fig. 8. At first a preliminary zero-offset section, which is equivalent to a conventional CMP stack section (automatic CMP stack), is generated. This stacked section is used to determine the wave-front attributes. Therefore, the quality of the automatic CMP stack determines the quality of the estimated attributes. In this first stage, the search parameter is the stacking velocity, $v_{\rm stk}$, which is given in terms of the CRS attributes as:

$$v_{\rm stk} = \left(\frac{2 v_0 R_{\rm NIP}}{t_0 \cos^2 \alpha_0} \right)^{\frac{1}{2}}. \qquad (2)$$

Vice versa, a stacking velocity field from conventional normal moveout analysis can be used as a minimum velocity limit for the automatic CRS parameter search, in order to avoid the stacking of multiples. However, multiples can also be alternatively suppressed by editing the CRS velocity (eq. 2), i.e. low-velocity zones which are attributed to multiples can be rejected. In the next two steps, the search parameters are α_0 and $R_{\rm N}$ (see e.g. Jäger *et al.* 2001; Menyoli 2002). The former is then used to compute $R_{\rm NIP}$ via eq. (2). With the optimum parameter triplet, the pre-stack data are stacked according to eq. (1) to give the final CRS stacked section.

5.1 Multifold stacking

A strength of the CRS stack method is its multifold stacking and its ability to produce the wavefield attributes. The multifold advantage is schematically shown in the CMP gather in Fig. 9. For small offsets, x the traveltime along the reflected CMP ray between source S_1 and receiver G_1 is approximated by the sum of the traveltime from S_1 to the NIP and from the NIP to G. Hubral & Krey (1980) showed that to second order and for small values of x the traveltime difference between a ray which traverses through S_1 NIP G_1 and the reflected CDP ray S_1 O G_1 can be neglected. Within this approximation, rays

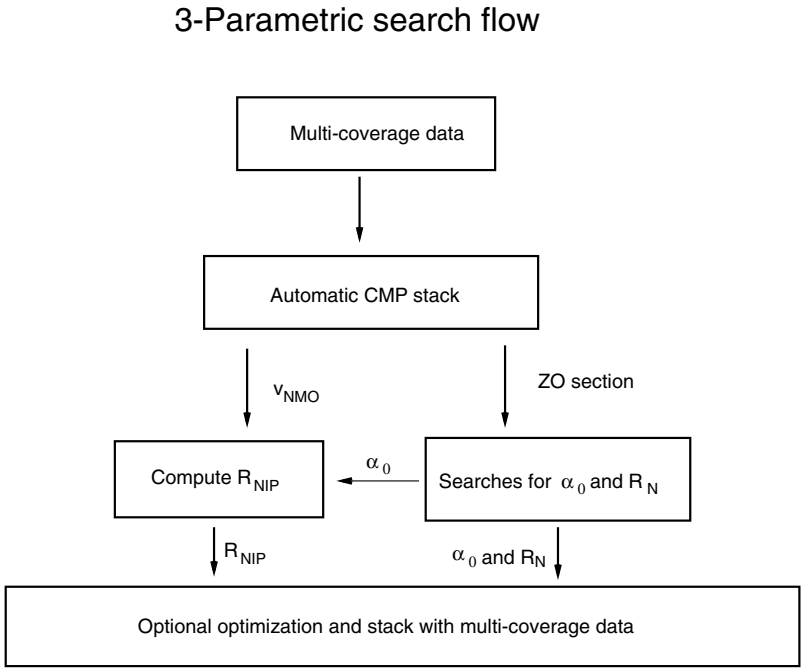

Figure 8. Simplified flowchart of the pragmatic approach for the determination of the CRS attributes according to Müller (1998).

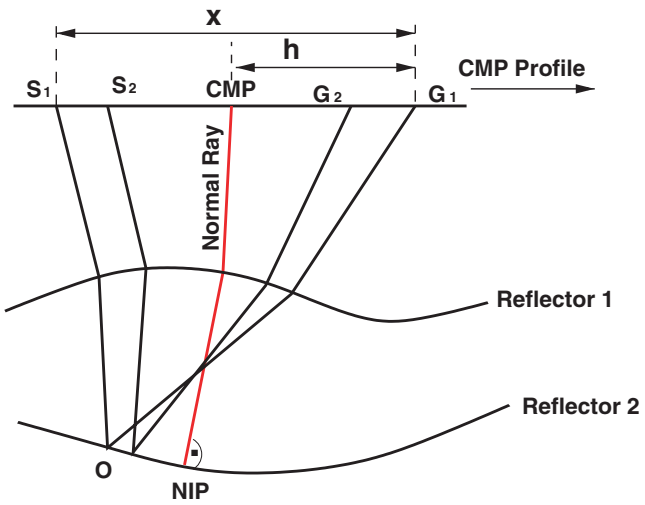

Figure 9. A 2-D curved layer model with a normal ray (central ray) and two CMP rays. The source–receiver separation is assumed small. The traveltime along the CMP ray S_1G_1 is approximated up to second order by the sum of the times from S_1 to NIP and from NIP to G_1 (Hubral & Krey 1980). Knowing the traveltimes of the normal ray, eq. (1) is used to approximate the traveltime from S_1 to the NIP, i.e. S_1 is in the vicinity of the normal ray. The same is also applied for the ray from NIP to G_1. In the CRS stack method the two-way times for the normal ray are picked for each time sample.

in the CMP gather can be associated with rays belonging to the hypothetical NIP wave front. Note that, there is a lateral displacement between the NIP from the actual reflection point. Likewise there is also a lateral displacement between the CMP ray reflection points across the reflector. Now, taking into account the NIP and N waves, traces from more than one CMP gather containing reflections associated with rays having the reflection point in the vicinity of NIP are considered for stacking. The summing of the corresponding amplitudes leads to multifold stacking. Therefore, depending on the distance of the lateral displacement ($x_m - x_0$) the CRS stacking operator (eq. 1) result in a greater stacking power compared with the classical CMP stack.

6 RESULTS AND DISCUSSIONS

The images of the selected areas in Fig. 5 are presented in Figs 6, 10 and 11. The results from the conventional CMP stacking are displayed on the top of these figures, whereas the results of the CRS stack are shown on the bottom. The CRS and CMP stack sections were migrated using the post-stack Kirchhoff algorithm. The stacking velocities obtained from CMP stacking were used as rms velocities for the migration. For comparison, the CRS stack and the CMP stack sections were migrated with the same rms velocities. In Fig. 6 the quality of the migrated CRS data is excellent compared with the CMP stack result. The S/N ratio is greatly improved and additional reflectors can be seen. The CRS stack in Fig. 6 is marked by a large number of continuous and highly energetic reflectors, which appeared weaker and less coherent in the CMP stack. The steeply dipping events (approximately 40°) that outcrop at the surface are imaged more clearly in the CRS result than in the obscured CMP image. We see significant differences between these migrated sections in the upper right portion of the sections where the change in reflector orientation near the surface indicates the outcrop of the main fault line. The surface location of this fault line was also seen in the structural geological section of the area. Coherent reflectors near the surface (TWT 0–0.7 s and trace numbers 0–210) which are not evident in the CMP stack of Fig. 6 are now imaged. The reflector continuity of the main back-thrusted reflector, between TWT 1.5 s and 2.2 s, is improved, which is important for estimating the amount of inversion.

The improved quality and reflector continuity of the migrated CRS stacked section is attributed to the increased fold which is implicitly incorporated into the CRS stacking operator. Stacking a larger number of traces spanning over many CMP gathers (supergather) increases the stacking power and the S/N ratio compared with the conventional CMP stack. Note that in conventional CMP processing the stacking power is defined by the number of traces in a CMP gather and, primarily, by the acquisition fold. In the CRS stack the number of traces to be stacked is determined by the user through the extent of the aperture (h and x_m). While DMO tries to remove reflection point dispersal so that conventional stacking should stack the traces constructively, CRS stacking does not need to remove reflection point dispersal. Instead the traces are summed over the surface which contains the reflection response of several reflection points. Therefore, the reflector surface over which the CMP rays are distributed is imaged. Since the imaging is based on the local radii of curvature of the reflector element, it directly preserves dipping events which is the key property of DMO correction. The preservation and enhancement of dipping events is clearly demonstrated in the bottom display of Fig. 6. However, stacking over more CMP traces raises the question of spatial resolution. Gurevich & Landa (2002) showed that there is no severe loss of spatial resolution typically attributed to supergather velocity analysis.

Fig. 10 presents migrated images of an area which cover the main anticline. The top display of Fig. 10 represents conventional stacking and migration while the bottom display of Fig. 10 shows the CRS stack. An obvious difference in the subsurface resolution can be observed. The most remarkable feature is the anticline flank which can be much better interpreted in the CRS result. The CRS stack, where the properties of the reflector are implicitly taken into account, strongly enhances the anticline boundaries and reveals other horizons that are not visible in the CMP image on the top of Fig. 10. The event between TWT 3 s and 4 s in the CRS image is completely absent in the CMP stack of Fig. 10. This anticline structure is assumed to be caused by salt tectonics in this area (Stovba & Stephenson 1999).

The increase of the S/N-ratio is more obvious in Fig. 11, where the deep subsurface structure can be more easily identified. This figure marks the northern syncline with mainly Carboniferous formations. A very strong increase in reflector continuity in the migrated CRS stack image is observed. As shown in the previous main anticline example, the dipping layers especially benefit from the CRS technique although the dip is fairly mild here. Such structural features would be considered as very appropriate for CMP processing. The increased continuity of reflectors and the enhanced S/N ratio, however, suggest the application of CRS technology even in such regions. Note that despite the good results, the data in these areas were not of optimum quality due to a number of technical shortcomings (shot positioning restrictions due to intensive coal mining and coverage difficulties).

In generating the CRS stack images, the only required model parameter is the near-surface velocity v_0. For the survey area an average value was estimated from field statics. Note that the image quality of the result does not depend on this average near-surface velocity. In marine environments v_0 is readily known since it is given as the water velocity. Because no velocity analysis is performed, errors which might be due to velocity interpretation and incorrect

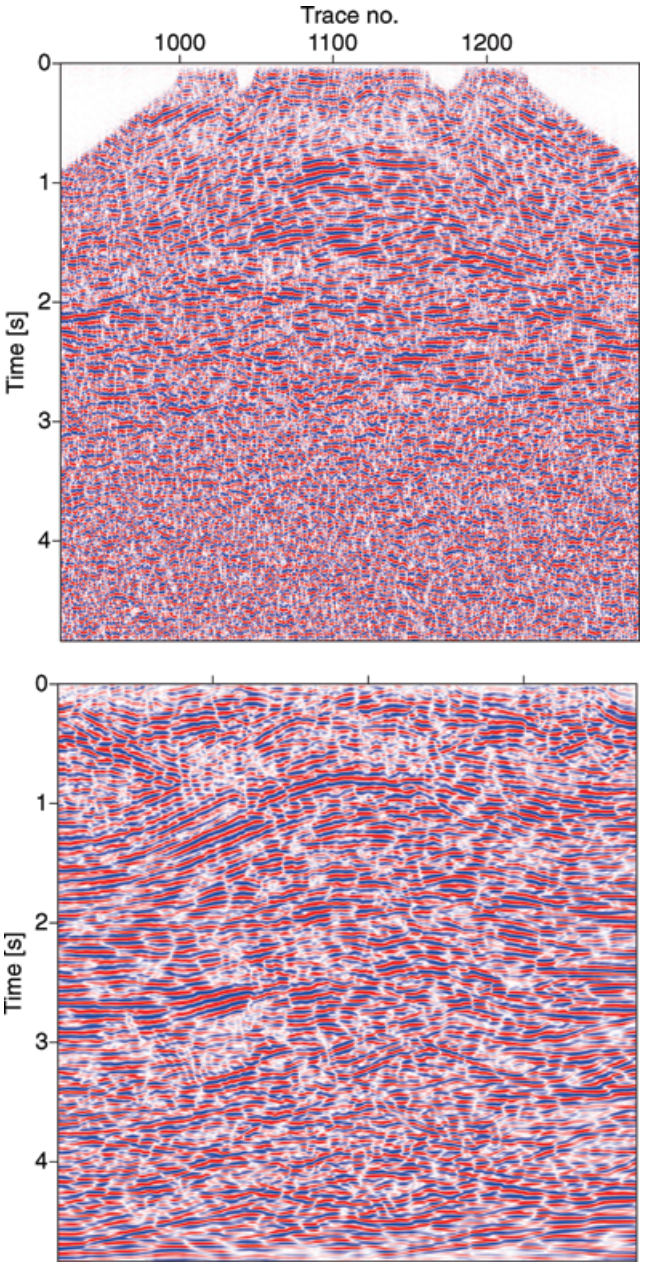

Figure 10. Post-stack time-migrated images of the main anticline after conventional CMP stacking (top) and after CRS stacking (bottom).

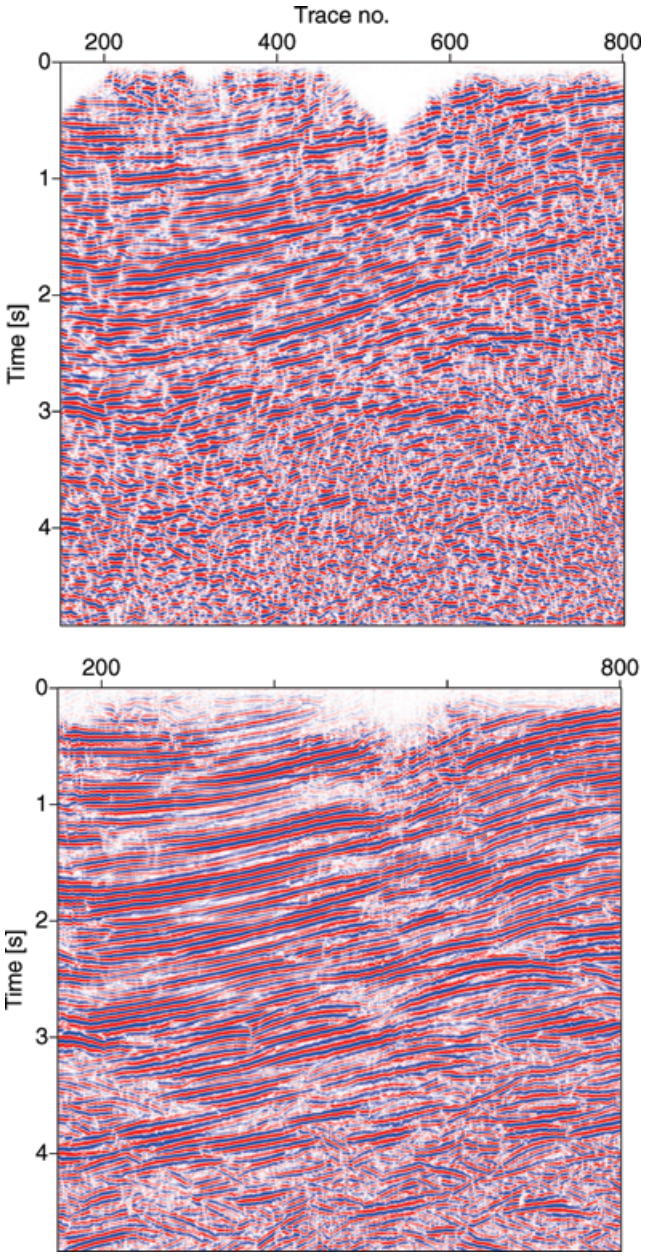

Figure 11. Post-stack time-migrated images after conventional CMP stacking (top) and after CRS stacking (bottom).

pre-stack event picking by the processor are avoided. The data-driven search strategy in the CRS could be of particular advantage for 3-D data. As shown in eq. (2) a high-resolution stacking velocity of the subsurface is also produced as a by-product (see Mann *et al.* 1999). Instead of using the rms velocity model from conventional methods for the post-stack migration, one can also use the CRS stacking velocity model to migrate the CRS stack images. For the data shown in this work the difference in the time-migrated images obtained from CMP and CRS velocities is only marginal. This emphasizes that the automatically obtained velocity model in the CRS procedure can be very valuable. A pre-stack Kirchhoff depth migration of the data with interval velocities derived from both the CMP and CRS velocities have shown unsatisfactory results. The image quality is considerably poorer than for the time-migrated CRS (i.e. post-stack) images. This, however, is attributed to problems in the velocity model. For pre-stack depth migration careful velocity building using migration velocity analysis is required (for more details see Menyoli 2002).

Fig. 12 shows the geological interpretation of the CRS image of Fig. 6. The interpretation was constrained by the surface structural geological section. The reflector continuity and the high S/N ratio simplified the interpretation of horizons. The interpretation shows a rifted Devonian basement, overlain by rifted and folded Carboniferous sediments. Note that the location of the fault lines on the surface was also observed on the surface structural geological section of the area. Because the basin in-fill was inverted in the Permian followed by erosion of younger sediments most of the sedimentary successions that outcrop right to the surface are of Carboniferous

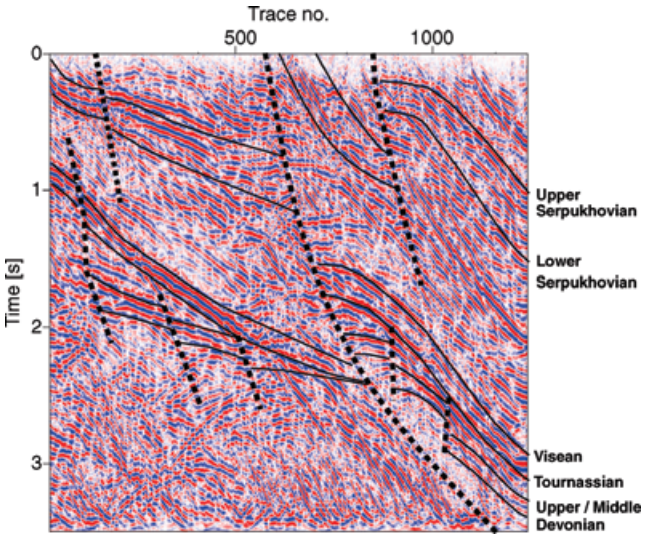

Figure 12. Geological interpretation of the CRS image in Fig. 6. This figure shows details of the basement involving a thrust on the southern flank of the foldbelt. The dotted lines are fault lines while the solid lines show reflection horizons.

age. The CRS results particularly support the interpretation of the inverted structures and enable determination of the total amount of inversion. This information is essential for palinspastic reconstruction (for more details on the geological modelling we refer to Maystrenko *et al.* 2003).

7 CONCLUSIONS

We have presented improved imaging results over the inverted structures and other complex areas of the Donbas Foldbelt. Standard preprocessing steps were used for the seismic data processing, while the model-independent CRS stack method and post-stack time migration were used to generate high-quality images. Because the CRS stack is purely data driven and no macrovelocity model is explicitly required, the use of a velocity model in the processing flow is 'postponed' until later stages like time or depth migration. Therefore, errors due to incorrect picking and interpretation of the stacking velocity model in such complex areas are reduced. The results of this experiment have shown that in complex areas CRS stacking and post-stack migration can produce high-quality images which are not achieved with conventional CMP stacking and the corresponding migration.

The high-quality stack is due to multifold advantage, i.e. stacking over more traces. Despite this stacking over more CMP gathers, spatial resolution can be maintained by controlling the extent of the summation aperture. For this data set, we have shown that the CRS stack has several advantages for producing unmigrated stacked sections. In particular the reflector continuity and S/N ratio is improved and due to the direct incorporation of the reflector dip in the summation process, dipping reflectors and reflector curvatures are preserved. High-quality time images are a pre-requisite for almost all model building techniques and migration velocity analysis. For complex areas CRS technology provides an alternative to conventional CMP processing. The good quality of the obtained images justifies the computational expense caused by the three-parametric search of the CRS attributes.

ACKNOWLEDGMENTS

This work was partly supported by the German Research Foundation (DFG, GA 350/9-1 and Ga 350/10-1), and the sponsors of the *Wave Inversion Technology (WIT) Consortium*. We kindly thank Dr Jürgen Mann (University of Karlsruhe) for providing the CRS stack code. Continuous discussions with the members of the Applied Geophysics Group Hamburg are highly appreciated. We are grateful to Ulf Bayer, Yuriy Maystrenko and Sergiy Stovba for providing the geological interpretation and to Randel Stephenson for setting up the international collaboration. Comments by P. Hubral, M. Korn and an anonymous reviewer are highly appreciated.

REFERENCES

Chekunov, A.V., Gavrish, V.K., Kutas, R.I. & Ryabchun, L.I., 1992. Dnieper-Donets paleorift. In: Geodynamics of rifting, Vol. I. Case history studies on rifts, Europe and Asia, ed. Ziegler, P.A., *Tectonophysics,* **208,** 257–272.

DOBREflection-2000 and DOBREfraction'99 Working Groups, 2000. DOBRE studies evolution of inverted intra-cratonic rifts in Ukraine, *EOS, Trans. Am. geophys. Un.,* **42,** 323–327.

Fertig, J., Thomas, M. & Thomas, R., 1999. How to remedy non-optimal seismic data by seismic processing, *Pure Appl. Geophys.,* **156,** 345–370.

Gelchinsky, B. & Keydar, S., 1999. Homeomorphic imaging approach: theory and practice, *J. appl. Geophys.,* **42,** 169–228.

Gelchinsky, B., Berkovitch, A. & Keydar, S., 1999. Multifocusing homeomorphic imaging: Part 1. Basic concepts and formulae, *J. appl. Geophys.,* **42,** 229–242.

Gurevich, B. & Landa, E., 2002. Multifocusing imaging with controlled reflection-point dispersal, *Geophysics,* **67,** 1586–1592.

Hubral, P., 1983. Computing true amplitude reflections in a laterally inhomogeneous Earth, *Geophysics,* **48,** 1051–1062.

Hubral, P. & Krey, Th., 1980. *Interval Velocities from Seismic Reflection Traveltime Measurements,* 203 pp. Society of Exploration Geophysicists, Tulsa, OK.

Jäger, R., Mann, J., Höcht, G. & Hubral, P., 2001. Common-reflection surface stack: image and attributes, *Geophysics,* **66,** 97–109.

Landa, E., Gurevich, B., Keydar, S. & Trachtman, P., 1999. Application of multifocusing method for subsurface imaging, *J. appl. Geophys.,* **42,** 283–300.

Mann, J., Jäger, R., Müller, T., Höcht, G. & Hubral, P., 1999. Common-reflection-surface stack—a real data example, *J. appl. Geophys.,* **42,** 301–318.

Maystrenko, Y. *et al.,* 2003. Crustal-scale pop-up structure in cratonic lithosphere: DOBRE deep seismic reflection study of the Donbas Foldbelt, Ukraine, *Geology,* **31,** 733–736.

Menyoli, E., 2002. Structural imaging in complex geological area: Integrating model-dependent and model-independent imaging, PhD Thesis, Part II, University of Hamburg, Germany.

Menyoli, E., Gajewski, D. & Hübscher, Ch., 2002. Time migrated CRS images of complex inverted basin structures, *72nd Annual International SEG Meeting, Expanded Abstracts,* pp. 2054–2057, Society of Exploration Geophysicists, Tulsa, OK.

Müller, T., 1998. Common reflection surface stack versus NMO/stack and NMO/DMO/stack, *60th Meeting of the European Association of Exploration Geohysicists, Houten, Extended Abstracts,* pp. 1–20.

Müller, T., 1999. The common reflection surface stack method-seismic imaging without explicit knowledge of the velocity model, Der Andere Verlag, Bad Iburg.

Perroud, H., Hubral, P. & Hoecht, G., 1999. Common-reflection-point stacking in laterally inhomogeneous media, *Geophys. Prospect.,* **47,** 1–24.

Stovba, S.M. & Stephenson, R.A., 1999. The Donbas Foldbelt: its relationship with the uninverted Donets segment of the Dniepr-Donets Basin, Ukraine, *Tectonophysics,* **313,** 59–83.

Stovba, S.M., Stephenson, R.A. & Kivshik, M., 1996. Structural features and evolution of the Dnieper-Donets Basin,Ukraine, from regional seismic reflection profiles, *Tectonophysics,* **268,** 127–147.

Trappe, H., Gierse, G. & Prüssmann J., 2001. Case studies show potential of common reflection surface stack-structural resolution in the time domain beyond the conventional NMO/DMO stack, *First Break,* **19,** 625–633.

Yan, L. & Line, L., 2001. Seismic imaging and velocity analysis for an Alberta Foothills seismic survey, *Geophysics,* **66,** 721–732.

Yilmaz, Ö., 2001. *Seismic Data Analysis: Processing, Inversion and Interpretation of Seismic Data,* Vols 2, eds Cooper, M.R. and Doherty, S.M., Society of Exploration Geophysicists, Tulsa, OK.